Electronic Supplementary Material (ESI) for Journal of Materials Chemistry A.

This copy of the ESI replaces the previous version published on 18 May 2023

Improving the Selectivity of Hydrogenation and Hydrodeoxygenation for Vanillin by Vacancy-Coupled Ru-N_3 Single Atoms Immobilized on Defective Boron Nitride

*Haoxiang Fan,[a, b, +] Fengjuan Qin,[a, +] Qi Yuan,[c, +] Zhiyi Sun,[a] Hongfei Gu,[a] Wenjing Xu,[a] Hao Tang,[a] Shuhu Liu,[d] Yu Wang,[e] Wenxing Chen,[a] Jia Li,[c, *] Huazhang Zhai,[a, b, *]*

[a] Energy & Catalysis Center, School of Materials Science and Engineering, Beijing Institute of Technology, Beijing 100081, China.

[b] Beijing Key Laboratory of Construction Tailorable Advanced Functional Materials and Green Applications, School of Materials Science, Beijing Institute of Technology, Beijing 100081, China

[c] Laboratory for Computational Materials Engineering, Division of Energy and Environment, Graduate School at Shenzhen, Tsinghua University, Shenzhen 518055, China.

[d] Beijing Synchrontron Radiation Facility, Institute of High Energy Physics, Chinese Academy of Science, Beijing 100029, China.

[e] Shanghai Synchrotron Radiation Facilities, Shanghai Institute of Applied Physics, Chinese Academy of Science, Shanghai 201204, China.

[*] Corresponding author. E-mail: huazhzhai@bit.edu.cn, lijia@phys.tsinghua.edu.cn

[+] These authors contributed equally to this work.

Table of contents

1. Materials
2. XAFS Data Process
3. Density Functional Theory
4. Supporting Figures and Tables

1. Materials.

Boric acid (H_3BO_3, 99.5%, Sanhe Branch of Beijing Tongguang Fine Chemical Company), Urea ($CO(NH_2)_2$, 99.0%, Sanhe Branch of Beijing Tongguang Fine Chemical Company), Methyl alcohol, anhydrous (CH_3OH, 99.5%, Sanhe Branch of Beijing Tongguang Fine Chemical Company), Ethanol (CH_3CH_2OH, AR, Sanhe Branch of Beijing Tongguang Fine Chemical Company), Ruthenium(Ⅲ)2,4-pentanedionate(Ru ($C_5H_7O_2)_3$, 98%), dicyandiamide (DCDA, HWRK CHEM), Trimesic acid ($C_9H_6O_6$, 98%, Jiangsu Aikon), Hexagonal Boron Nitride (h-BN, 99.9%, psaitong). The deionized water used in all experiments was obtained through ion-exchange and filtration. All the chemicals were analytical grade and used without further purification.

2. XAFS Data Process

The acquired EXAFS data were processed according to the standard procedures using the Athena and Artemis implemented in the IFEFFIT software packages. The fitting detail is described below:

The acquired EXAFS data were processed according to the standard procedures using the ATHENA module implemented in the IFEFFIT software packages. The EXAFS spectra were obtained by subtracting the post-edge background from the overall absorption and then normalizing with respect to the edge-jump step. Subsequently, the χ(*k*) data of were Fourier transformed to real (R) space using a hanning windows (dk=1.0 $Å^{-1}$) to separate the EXAFS contributions from different coordination shells. To obtain the quantitative structural parameters around central atoms, least-squares curve parameter fitting was performed using the ARTEMIS module of IFEFFIT software packages.

The following EXAFS equation was used:

$$\chi(k) = \sum_j \frac{N_j S_o^2 F_j(k)}{kR_j^2} exp[-2k^2\sigma_j^2] exp[\frac{-2R_j}{\lambda(k)}] sin[2kR_j + \phi_j(k)]$$

S_0^2 is the amplitude reduction factor, $F_j(k)$ is the effective curved-wave backscattering amplitude, N_j is the number of neighbors in the j^{th} atomic shell, R_j is the distance between the X-ray absorbing central atom and the atoms in the j^{th} atomic shell (backscatterer), λ is the mean free path in Å, $\varphi_j(k)$ is the phase shift (including the phase shift for each shell and the total central atom phase shift), σ_j is the Debye-Waller parameter of the j^{th} atomic shell (variation of distances around the average R_j). The functions $F_j(k)$, λ and $\varphi_j(k)$ were calculated with the ab initio code FEFF8.2. The coordination numbers of model samples were fixed as the nominal values. The obtained S_0^2 was fixed in the subsequent fitting. While the internal atomic distances R, Debye-Waller factor σ^2, and the edge-energy shift ΔE_0 were allowed to run freely.

2.Density Functional Theory

In DFT calculation，five kinds 7 × 7 × 1 boron nitride (BN) monolayer with Ru doped were construct to investigate the hydrogenation and hydrodeoxygenation of vanillin. Five unique doping sites are found as shown in Figure S23(a to e). one 7 × 7 × 1 graphene monolayer with one Ru and three nitrogen (Ru bond with three nitrogen) doped and one 3 × 3 × 1 g-C_3N_4 with one Ru doped as contrast model to investigate the hydrogenation and hydrodeoxygenation of vanillin. Two models are found as shown in Figure S23(f) and (g).

The structure parameters and the binding energy of Ru in different sites are showed in Table S5. The binding energy was calculated by using $E_b = E_{total} - E_{substrate} – E_{Ru}$ equation. Where E_{total}, $E_{substrate}$ and E_{Ru} indicate the energies of the adsorbate supported substrate, pure substrate without Ru combining, the energy of a Ru atom in a big cell, respectively. In order to determine which structure is the active site for the hydrogenation of vanillin, the adsorption energies of the horizontal (figure S24) and vertical (figure S25) vanillin were calculation on boron nitride, graphene and g-C_3N_4. On boron nitride surface, four unique horizontal vanillin were considered. The most stable structure is Ru-SA/h-BN-1 which only O in aldehyde bond with Ru and the benzene ring on the top of nitrogen atom. Ru-SA/h-BN-3 is both O and C in aldehyde bond with Ru. The adsorption energies of the horizontal vanillin on Ru-N_3, Ru-SA/NC-V_C and Ru-SA/C_3N_4 are -1.979, -2.011 and -2.119, which is lower than vertical vanillin on each surface. This means the horizontal vanillin is most stable on Ru-N_3, Ru-SA/NC-V_C and Ru-SA/C_3N_4 due to the van der waals interaction between vanillin and surface. To further investigate the hydrogenation of vanillin, the vacancy with one N was removed near Ru site was considered. The adsorption energy of vanillin in Ru-SA/pBN-V_N-2(Figure S24 (f)) is -2.204eV, which is lower than Ru-SA/pBN-V_N-1. This means the vacancy improve the combination of vanillin on boron nitride. The adsorption energy (E_{ads}) was computed along with the equation: $E_{ads} = E_{sur+vanillin} – E_{sur} – E_{vanillian}$. Where $E_{sur+vanillin}$, E_{sur}, and $E_{vanillian}$ indicate the energies of the vanillin adsorbed on the substrate, substrate with Ru combining, and vanillin which was in a big cell.

1. Supporting Figures and Tables

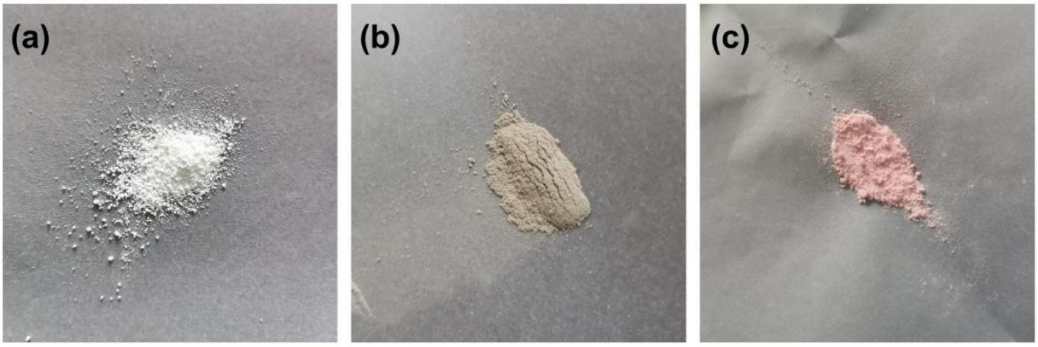

Figure S1. Digital photographs of pBN(a), Ru-SA/pBN-V_N (b) and $Ru(acac)_3$/pBN-V_N before calcine(c), respectively.

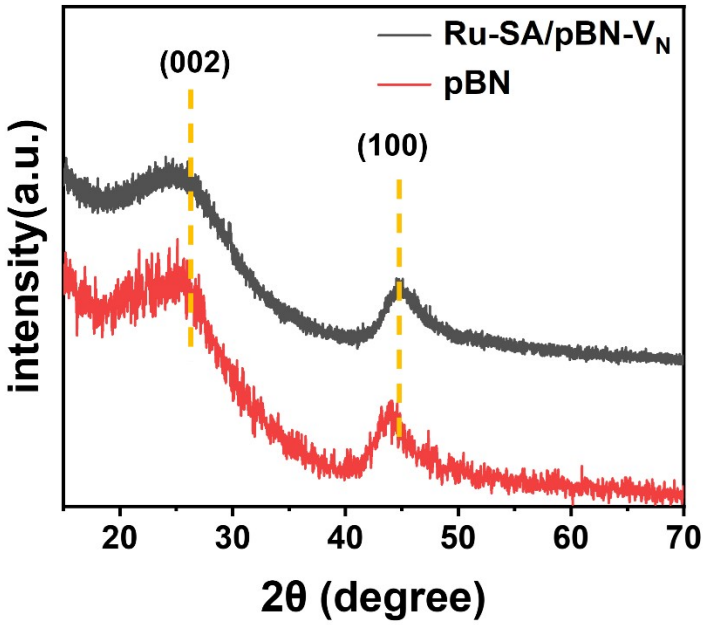

Figure S2. XRD patterns of pBN and Ru-SA/pBN-V_N.

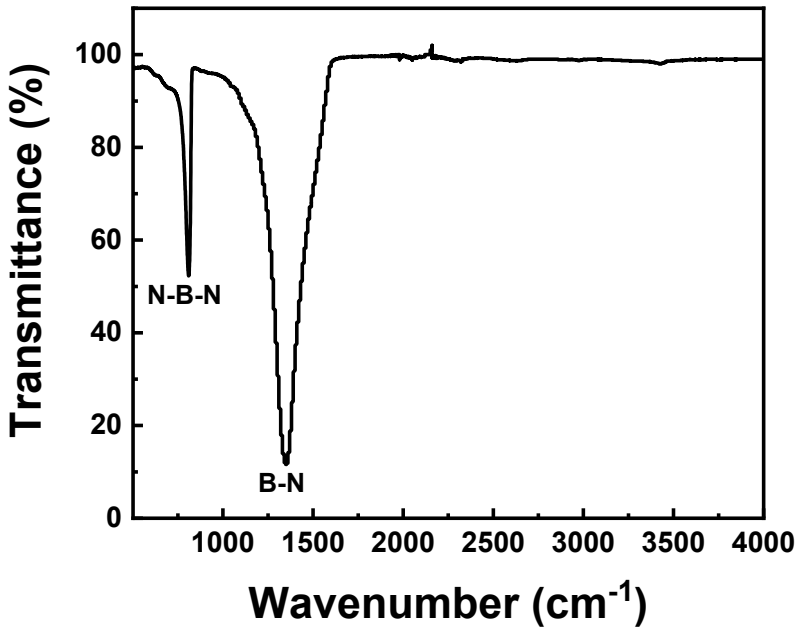

Figure S3. The FT-IR spectrum of pBN.

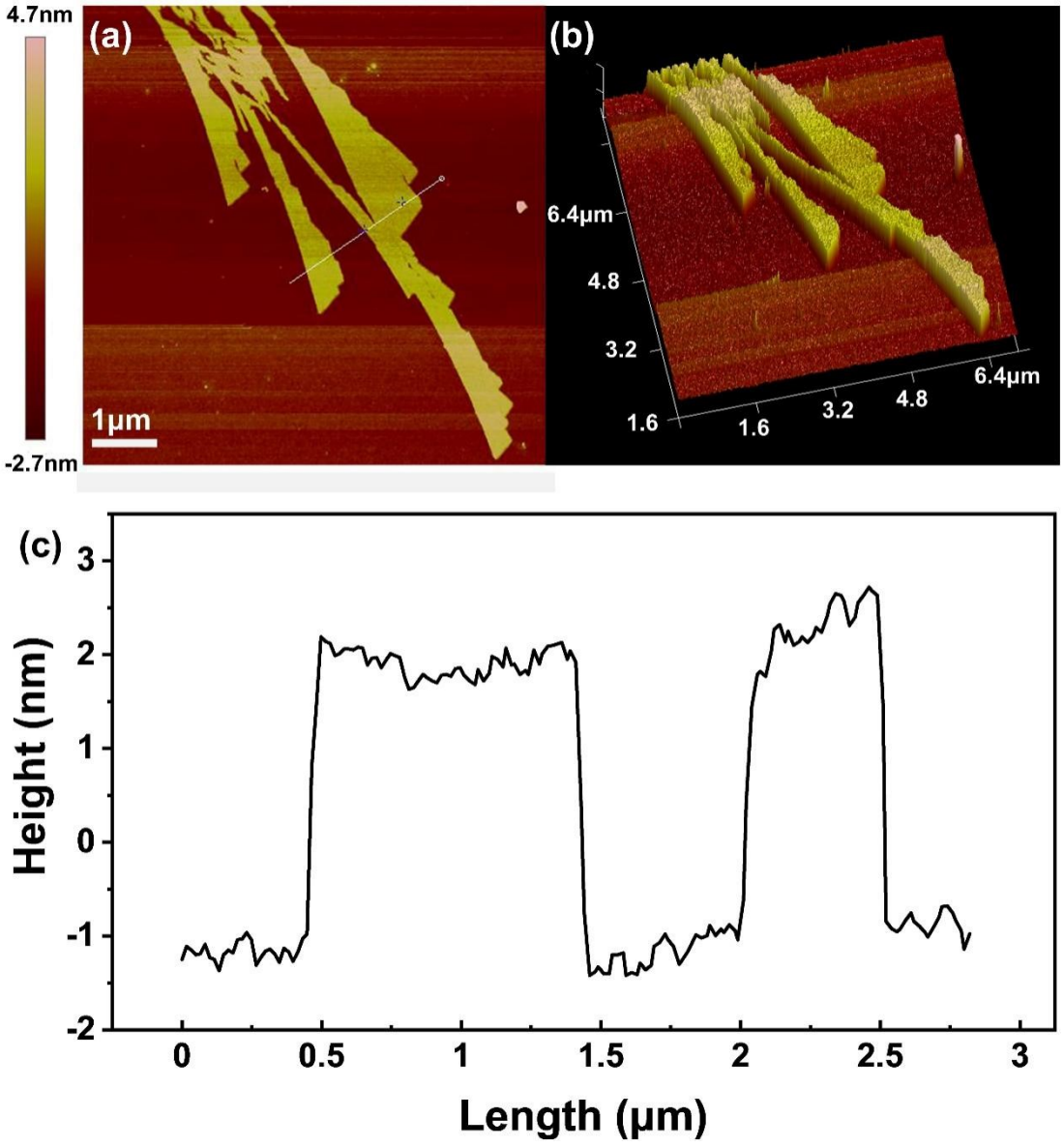

Figure S4. AFM image of amorphous pBN. (a) AFM photo; (b) Schematic diagram; (c) Sample thickness map in selected direction.

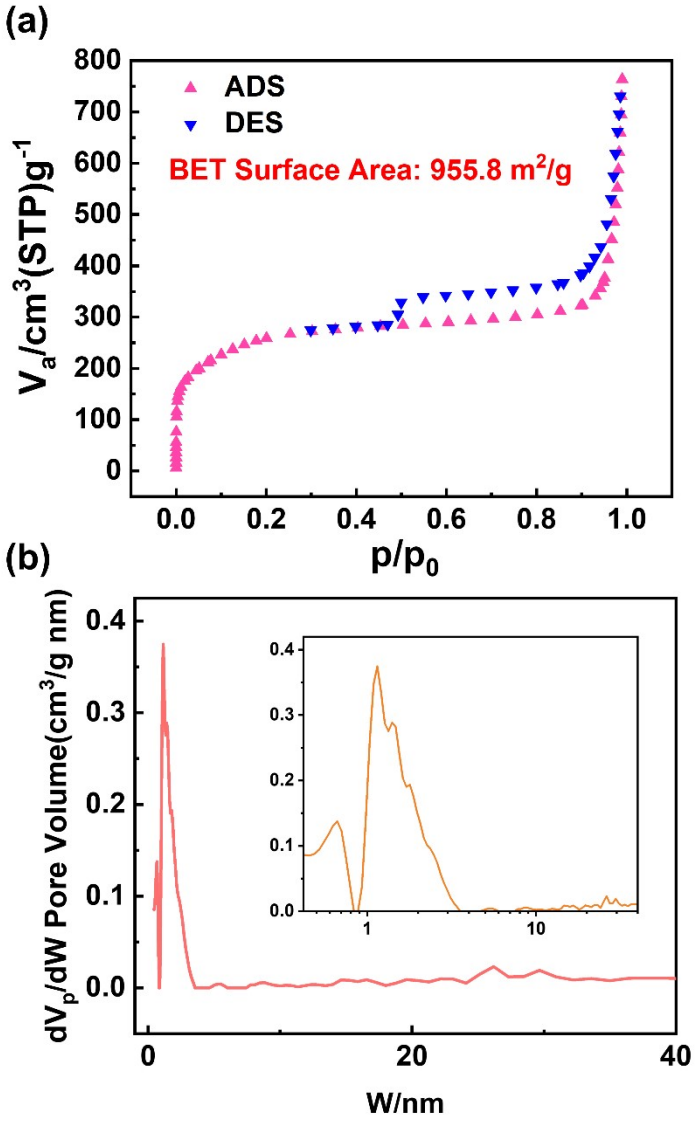

Figure S5. BET surface area and pore size distribution. N_2 adsorption-desorption isotherms(a) and pore-size distribution(b) of pBN. BET surface area of is 955.8 m^2/g.

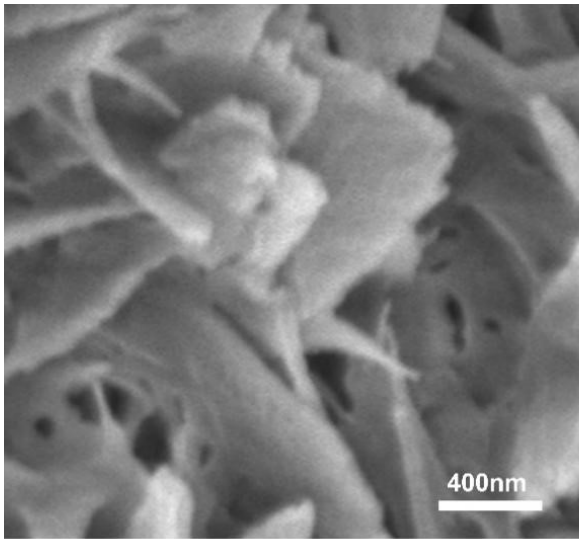

Figure S6. SEM images of Ru-SA/pBN-V_N.

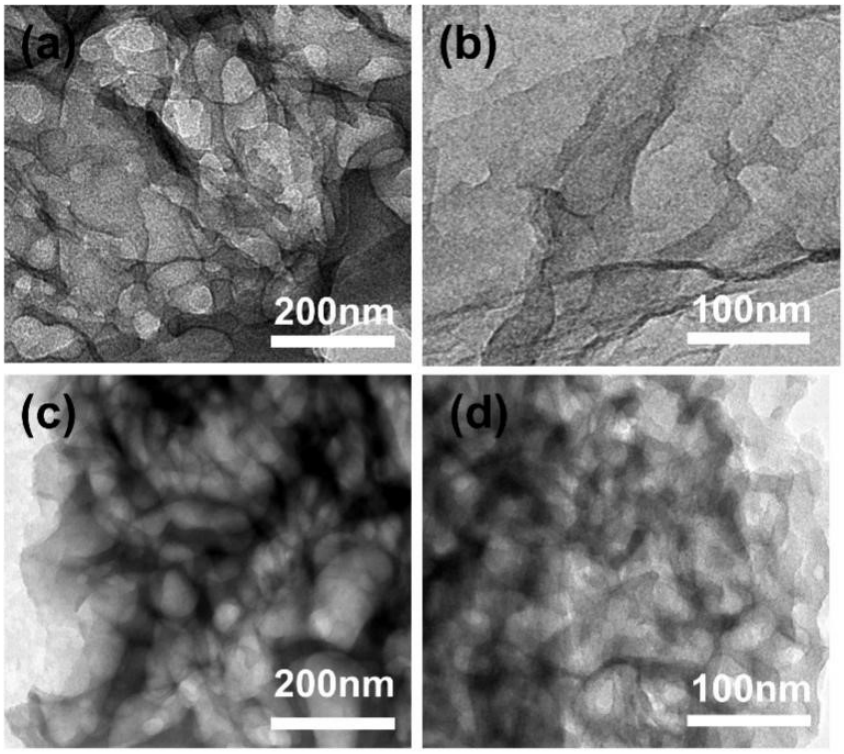

Figure S7. TEM images of Ru-SA/pBN-V_N at different area.

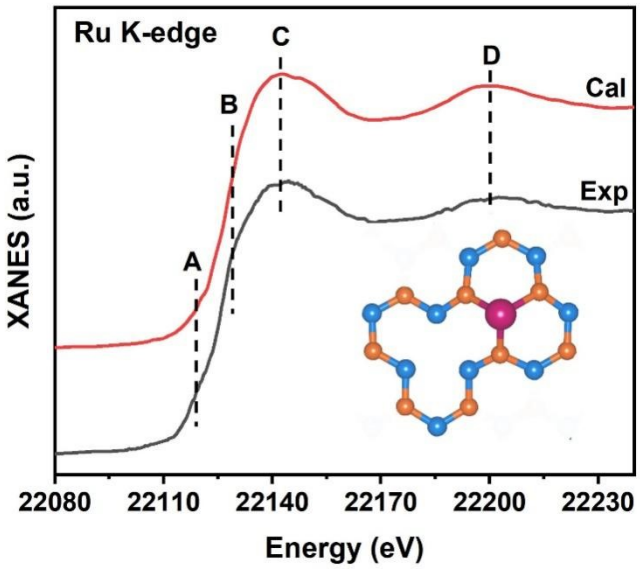

Figure S8. The simulated XANES spectrum based on the instead atomic interface structure, compared with the experimental spectrum of Ru-SA/pBN-V_N. The Ru K-edge theoretical XANES simulations were carried out with the FDMNES code in the framework of real-space full multiple-scattering (FMS) scheme using Muffin-tin approximation for the potential. The energy dependent exchange-correlation potential was calculated in the real Hedin-Lundqvist scheme, and then the spectra convoluted using a Lorentzian function with an energy-dependent width to account for the broadening due both to the core-hole width and to the final state width.

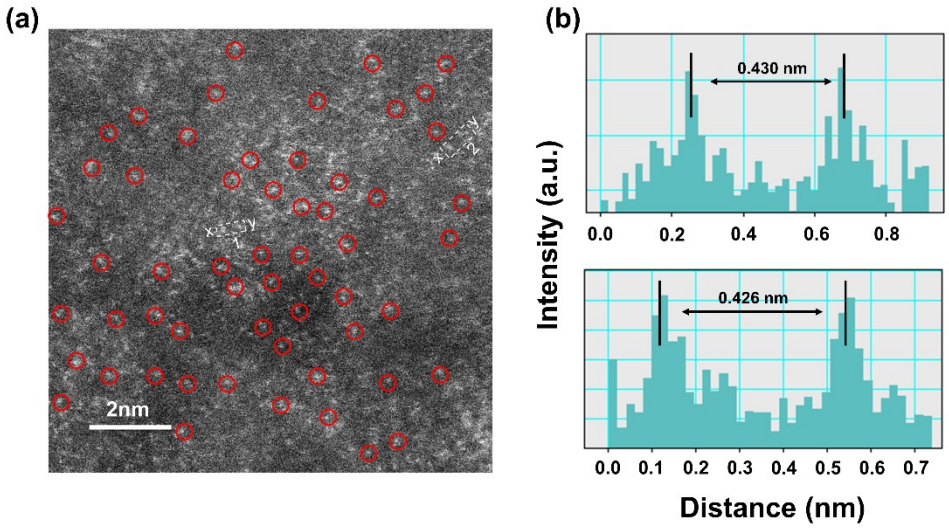

Figure S9. (a) AC-HAADF-STEM images of Ru-SA/h-BN. (b) The corresponding intensity profiles along the line X-Y in **a**.

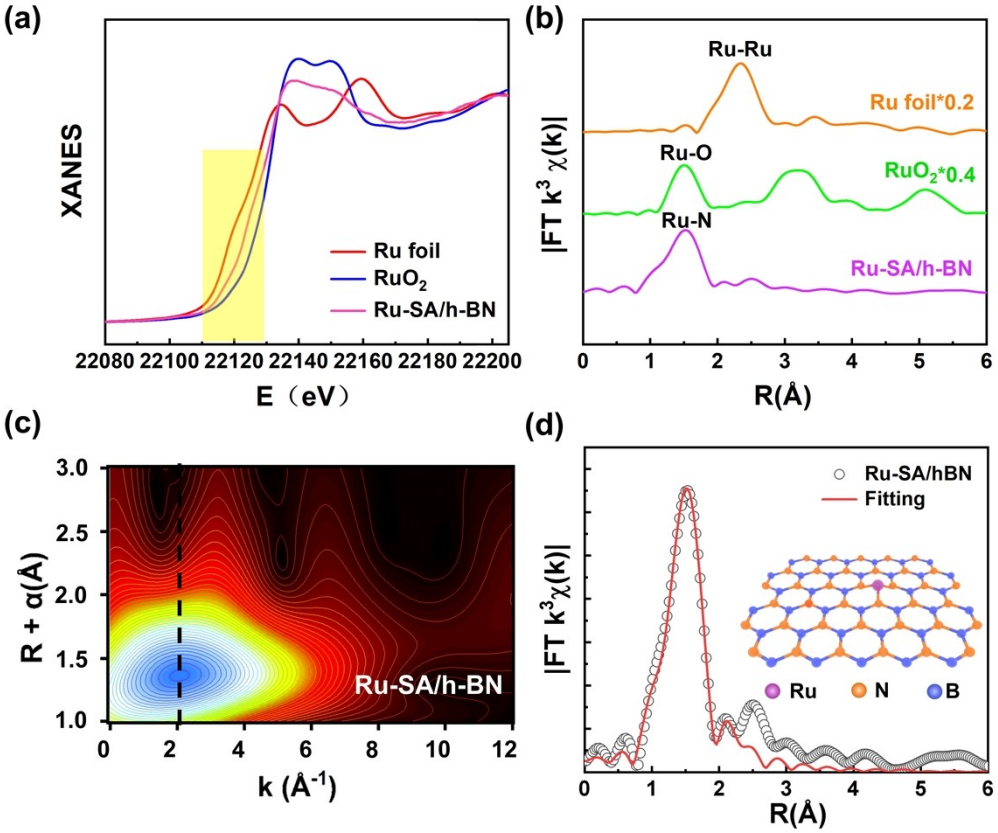

Figure S10. (a) XANES and (b) FT-EXAFS spectra of Ru-SA/h-BN. (c) WT-EXAFS plots of Ru-SA/h-BN. (d) The EXAFS fitting curves of Ru-SA/h-BN.

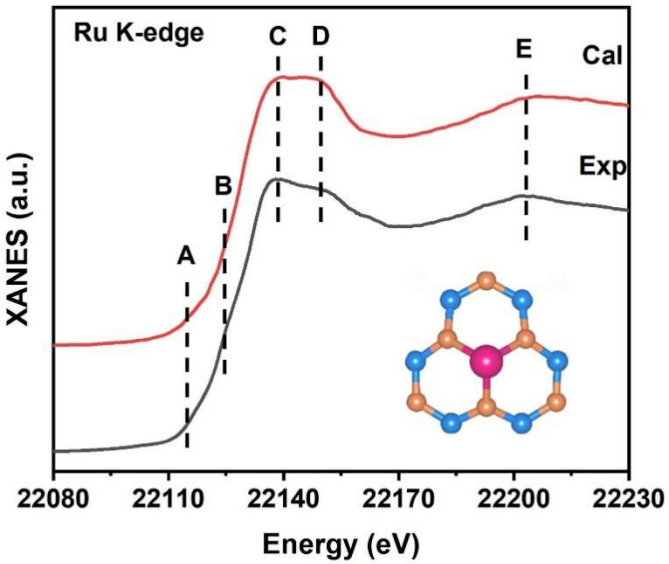

Figure S11. The simulated XANES spectrum based on the instead atomic interface structure, compared with the experimental spectrum of Ru-SA/h-BN.

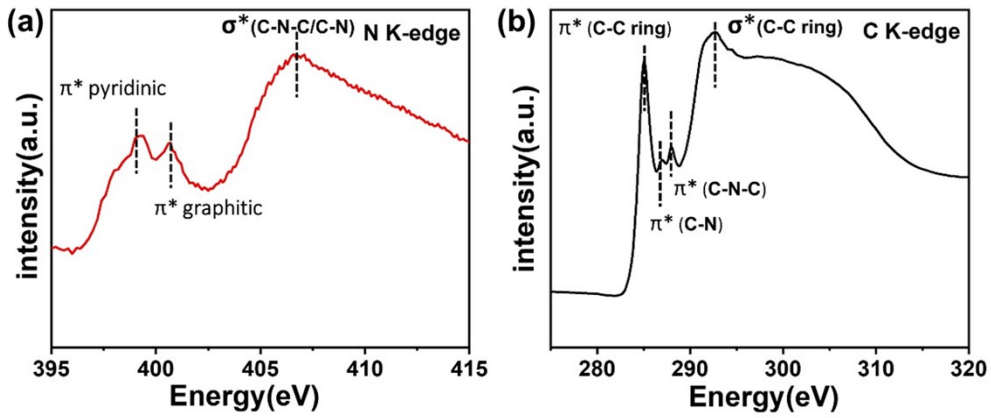

Figure S12. (a) Nitrogen and (b) carbon K-edge NEXAFS spectra of NC.

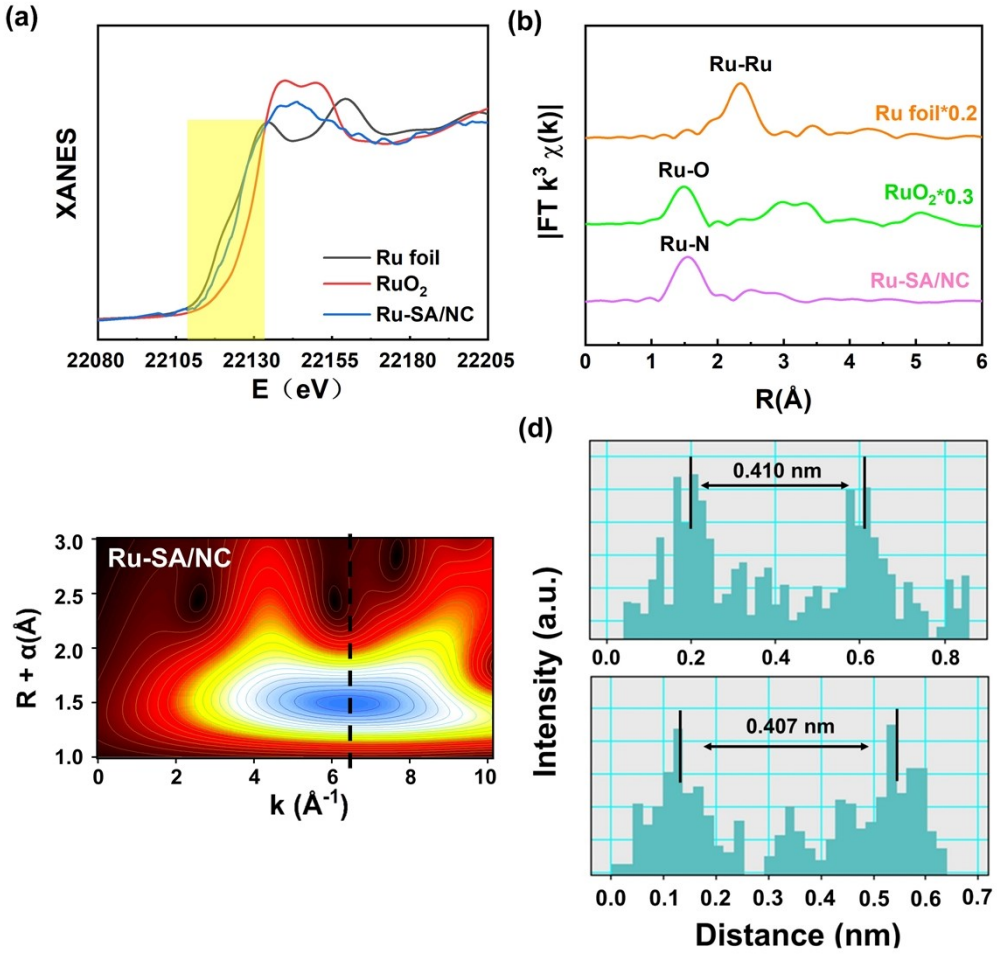

Figure S13. (a) XANES and (b) FT-EXAFS spectra of Ru-SA/NC. (c) WT-EXAFS plots of Ru-SA/NC. (d) The corresponding intensity profiles along the line X-Y in Fig 4b.

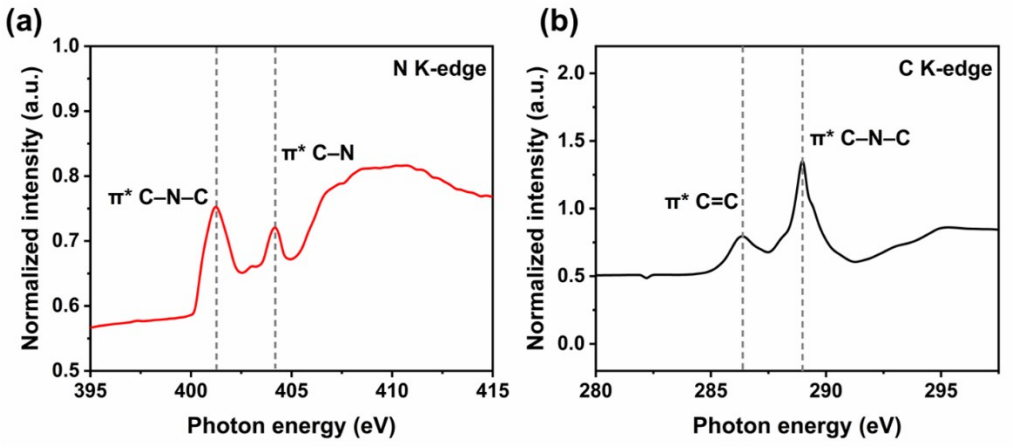

Figure S14. (a) Nitrogen and (b) carbon K-edge NEXAFS spectra of C_3N_4.

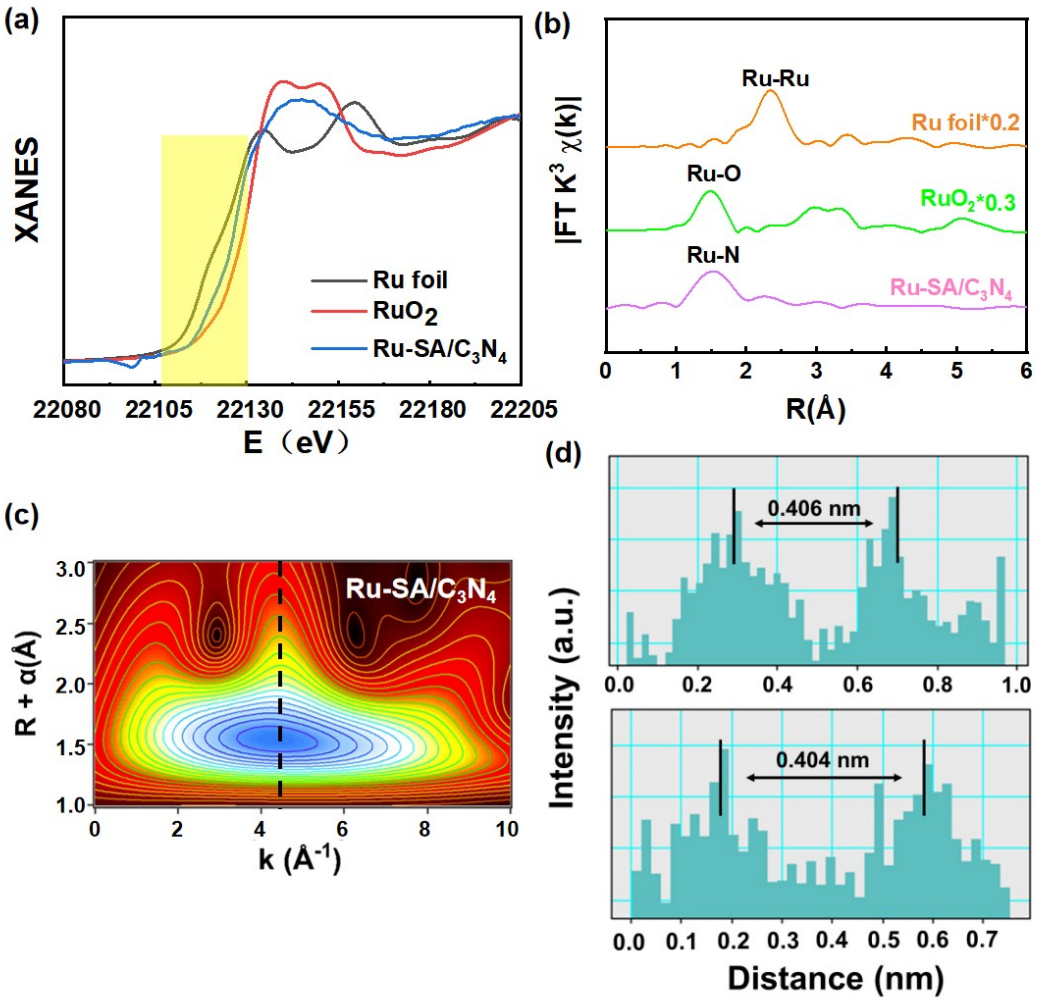

Figure S15. (a) XANES and (b) FT-EXAFS spectra of Ru-SA/C_3N_4. (c) WT-EXAFS plots of Ru-SA/C_3N_4. (d) The corresponding intensity profiles along the line X-Y in Fig 4e.

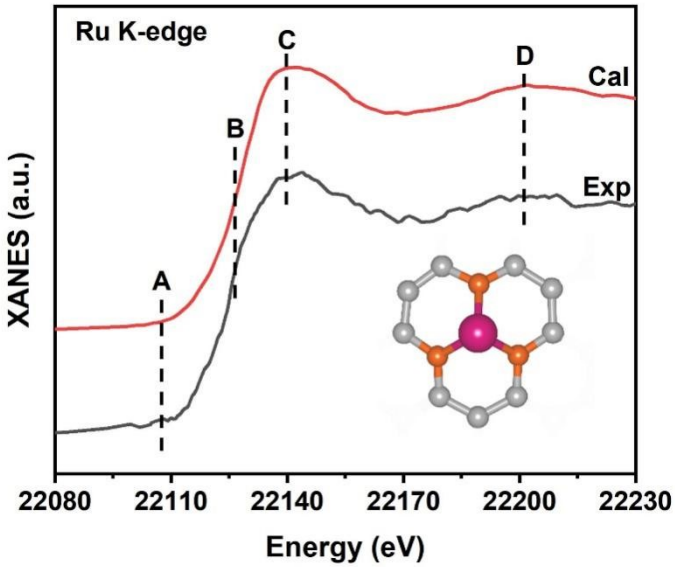

Figure S16. The simulated XANES spectrum based on the instead atomic interface structure, compared with the experimental spectrum of Ru-SA/NC.

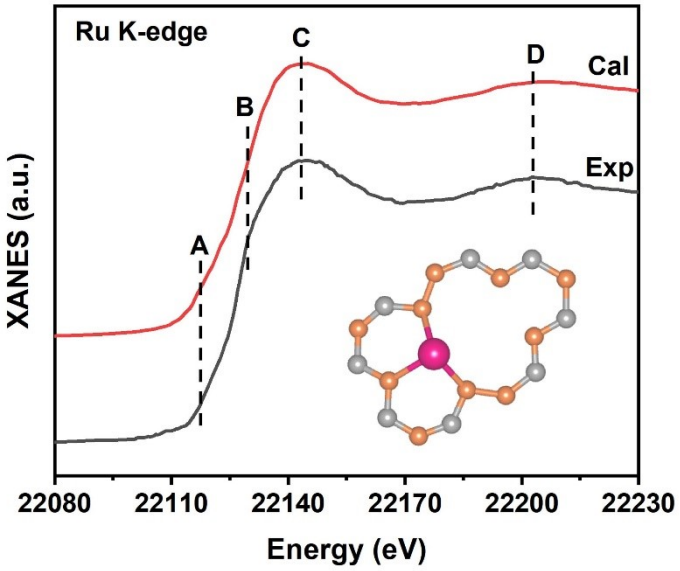

Figure S17. The simulated XANES spectrum based on the instead atomic interface structure, compared with the experimental spectrum of Ru-SA/C_3N_4.

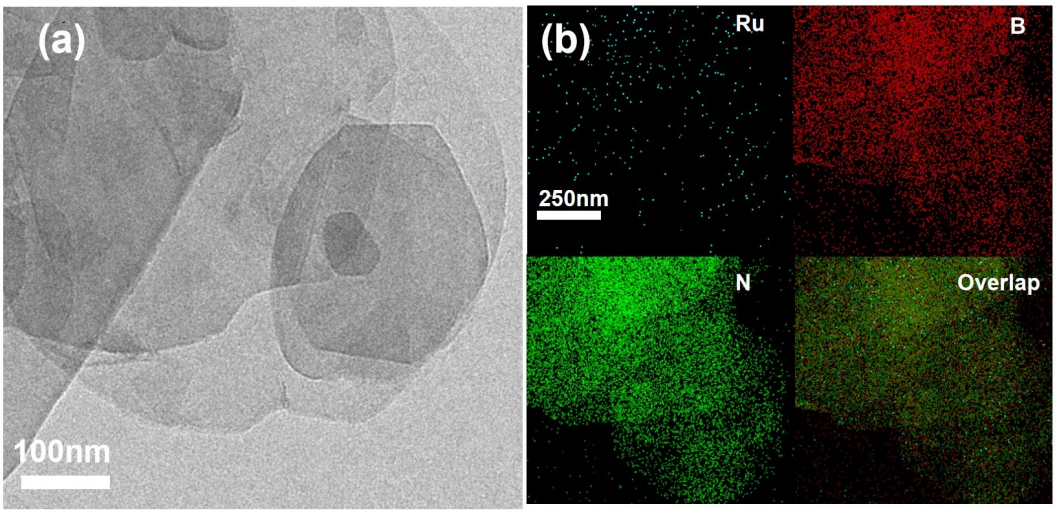

Figure S18. XRD patterns of the as-prepared Ru-SA/pBN-V_N, Ru-SA/pBN-V_N after five times recycle of hydrogenation and Ru-SA/pBN-V_N after five times recycle of hydrodeoxygenation.

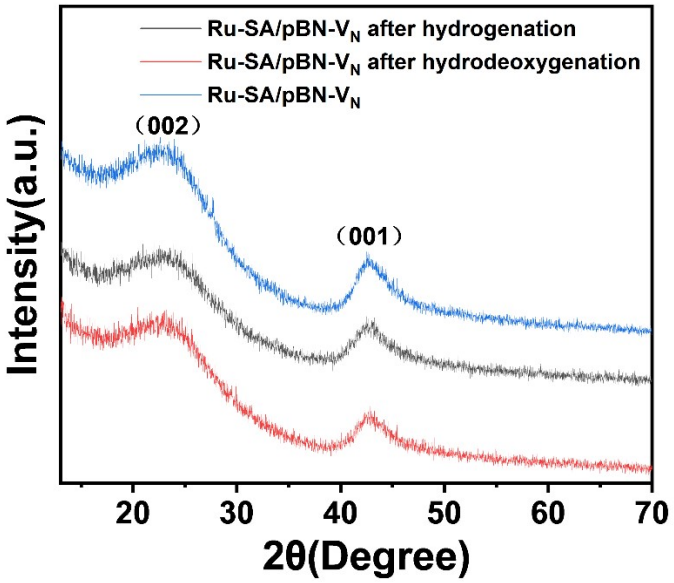

Figure S19. XRD patterns of the as-prepared Ru-SA/pBN-V_N, Ru-SA/pBN-V_N after five times recycle of hydrogenation and Ru-SA/pBN-V_N after five times recycle of hydrodeoxygenation.

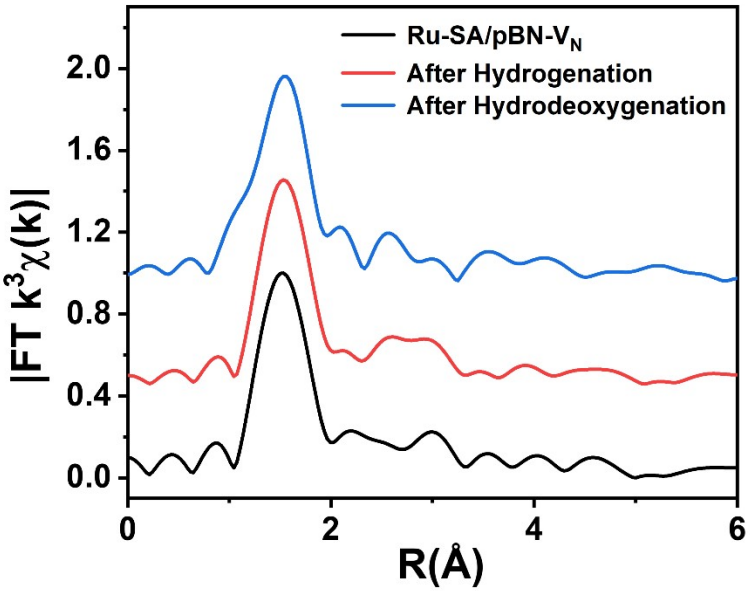

Figure S20. The EXAFS Fourier transformed (FT) k^3 –weighted χ(k)-function spectra of the Ru-SA/pBN-V_N catalyst before and after hydrogenation or hydrodeoxygenation reaction.

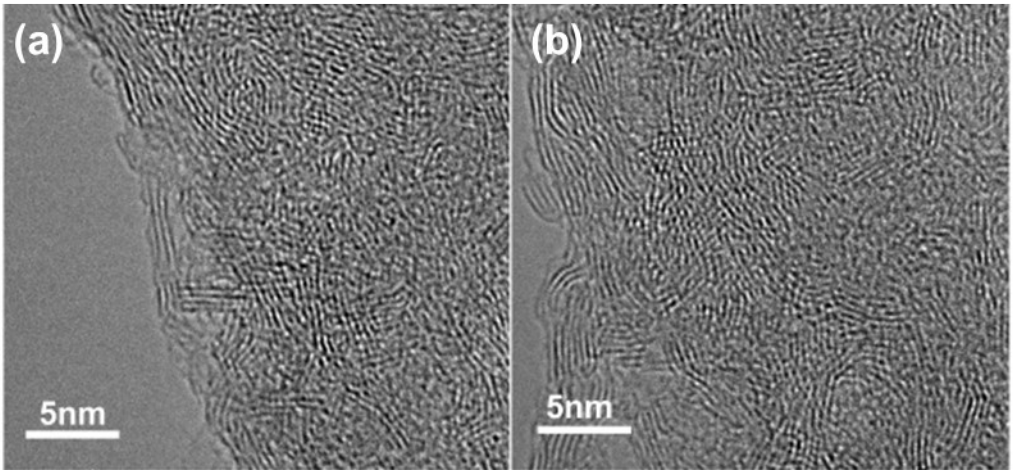

Figure S21. FE-TEM images of Ru-SA/pBN-V_N after five times recycle of (a) hydrogenation and (b) hydrodeoxygenation.

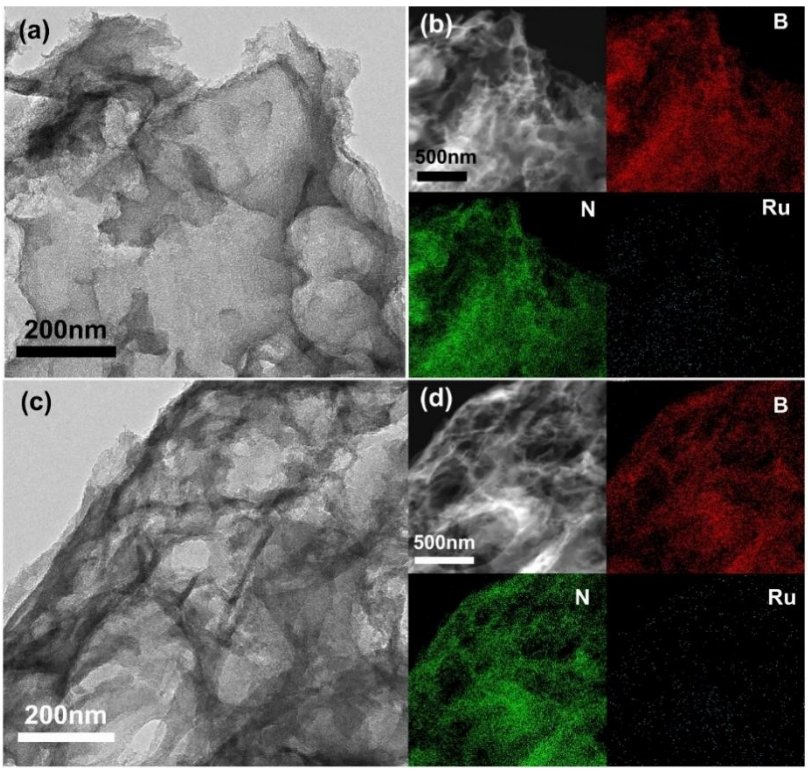

Figure S22. (a) HAADF-STEM and (b) the corresponding EDS images of Ru-SA/pBN-V_N after five times recycle of hydrogenation. (c) HAADF-STEM and (d) the corresponding EDS images of Ru-SA/BN after five times recycle of hydrodeoxygenation.

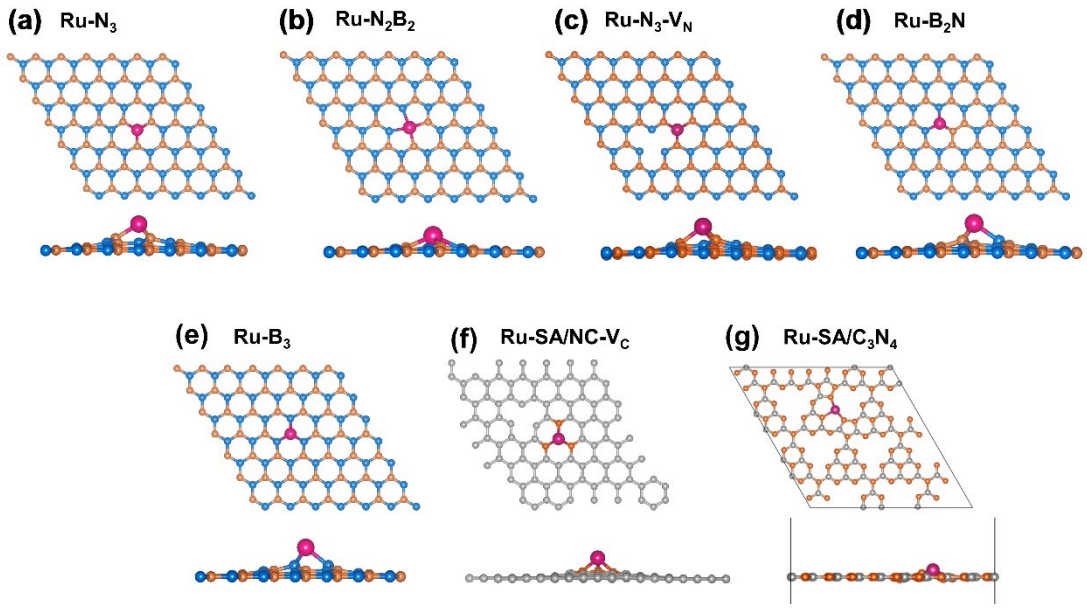

Figure S23. Top and side views for possible coordination structures of Ru on different vacancy, as well as the relative binding energies and bond length.

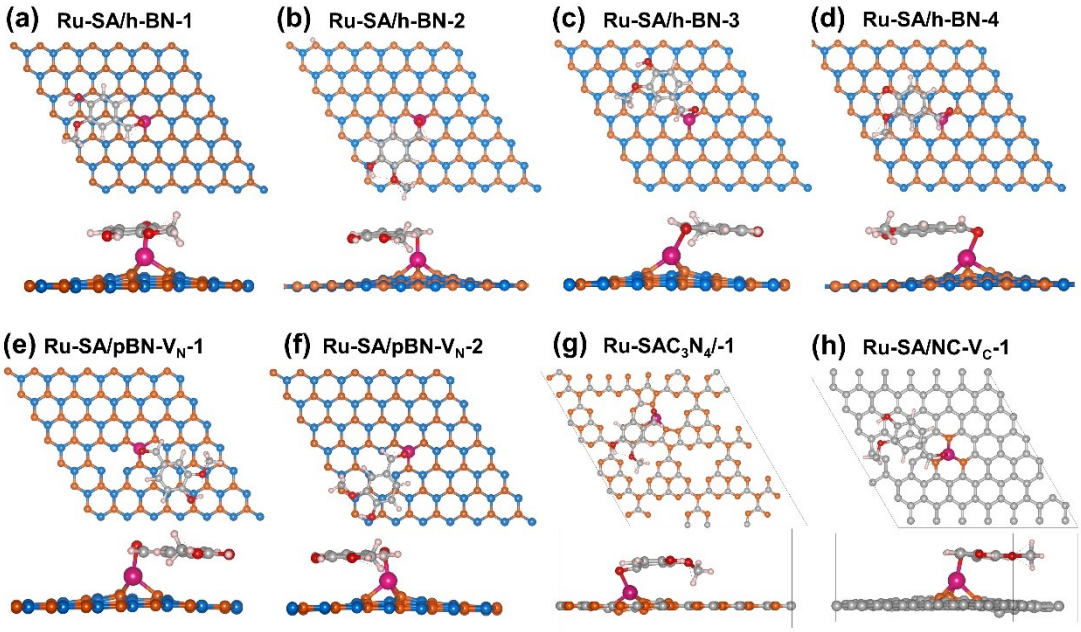

Figure S24. Top and side views for different configurations of vanillin on the carriers and adsorption energy.

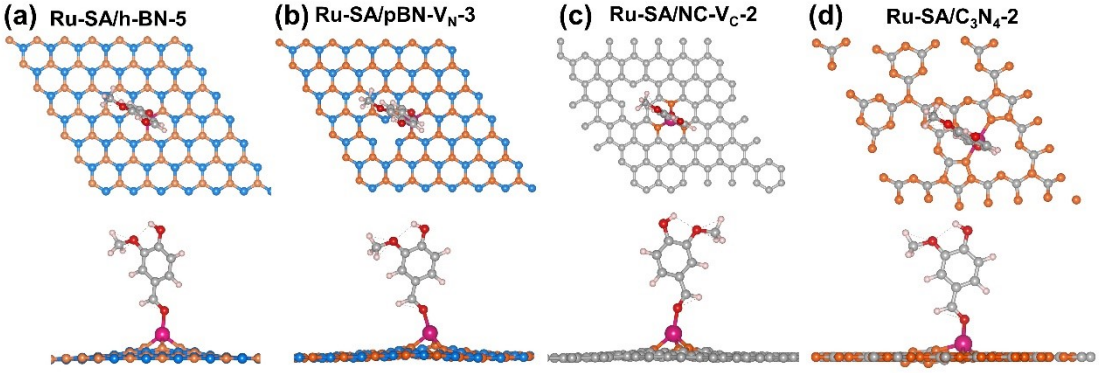

Figure S25. Top and side views for different configurations of vanillin on the carriers and adsorption energy.

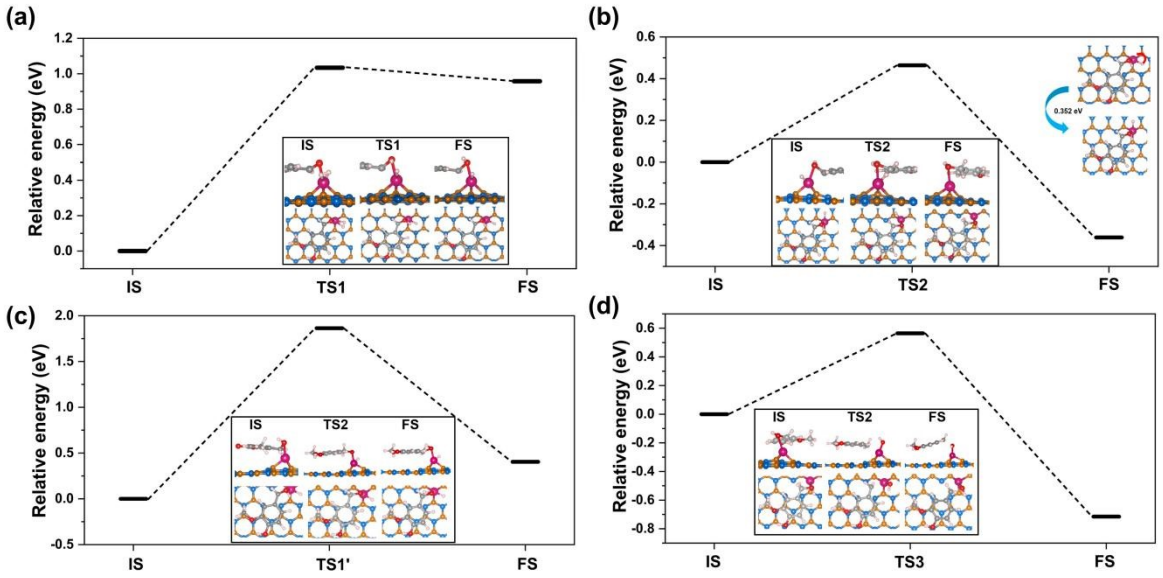

Figure S26. NEB calculation in hydrogenation. (a), (b) and (d) shows the barrier in Fig. S7a. (c) show the pathway from CH-HO* to CH_2O*, and it has proved that H which bonded with O hard to transfer to C to form CH_2O* because of high barrier (up to 1.8 eV). So the other hydrogen which was bonded to Ru was transfer to other site and also bonded with Ru.

Table S1. Structural parameters extracted from the Ru K-edge EXAFS fitting. (S_0^2=0.85).

Sample	Scattering pair	CN	R(Å)	σ^2(10^{-3}Å^2)	ΔE_0(eV)	R factor
Ru-SA/pBN-V_N	Ru-N_1	2.0	1.91	4.5	1.0	0.004
	Ru-N_2	1.2	1.94	5.8	1.0	
Ru-SA/h-BN	Ru-N	3.1	1.97	5.7	2.0	0.006
Ru-SA/C_3N_4	Ru-N_1	2.1	1.93	4.1	2.0	0.007
	Ru-N_2	1.3	1.96	4.8	2.0	0.004
Ru-SA/NC	Ru-N	3.1	1.95	4.6	1.5	0.006
Ru foil	Ru-Ru	12*	2.70	5.2	0.5	0.005

S_0^2 is the amplitude reduction factor; CN is the coordination number; R is interatomic distance (the bond length between central atoms and surrounding coordination atoms); σ^2 is Debye-Waller factor (a measure of thermal and static disorder in absorber-scatterer distances); ΔE_0 is edge-energy shift (the difference between the zero kinetic energy value of the sample and that of the theoretical model). R factor is used to value the goodness of the fitting.

Error bounds that characterize the structural parameters obtained by EXAFS spectroscopy were estimated as N ± 20%; R ± 1%; σ^2 ± 20%; ΔE_0 ± 20%.

* This value was fixed during EXAFS fitting, based on the known structure of Ru foil.

Table S2: Hydrogenation and Hydrodeoxygenation of Vanillin at Different Temperatures.

Catalyst	Temp (℃)	Time (h)	Conv (%)	Selectivity (%)	
				Vanillyl Alcohol	2-methoxy-p-cresol
Ru-SA/pBN-V_N	20	48	-	-	-
	40	48	20	~100	0
	60	24	95	~100	0
	80	6	25	67	33
	100	6	68	23	77
	120	6	~100	0	~100
	140	6	~100	0	~100

4 MPa H_2. TOF = 27 h^{-1}; TON = 638 (at 60 ℃); TOF=112 h^{-1}; TON = 673 (at 120 ℃)

Table S3. The hydrogenation and hydrodeoxygenation of vanillin at different Temperatures.

Catalyst	Temp (℃)	Time (h)	Conv (%)	Selectivity (%)	
				Vanillyl Alcohol	2-methoxy-p-cresol
	20	48	-	-	-
	40	48	15	~100	0
	60	24	44	~100	0
Ru-SA/h-BN	80	6	21	70	30
	100	6	30	29	71
	120	6	35	26	74
	140	6	43	23	77

4 MPa H_2. TOF = 13 h^{-1}; TON = 317 (at 60 ℃); TOF=42 h^{-1}; TON = 253 (at 120 ℃)

Table S4. The hydrogenation and hydrodeoxygenation of vanillin at different catalysts.

Catalyst	Temp (℃)	Time (h)	Conv (%)	Selectivity (%)	
				Vanillyl Alcohol	2-methoxy-p-cresol
Ru-SA/pBN-V_N	60	24	95	~100	0
	120	6	~100	0	~100
Ru-SA/h-BN	60	24	44	~100	0
	120	6	35	26	74
Ru-SA/NC	60	24	46	~100	0
	120	6	35	21	79
Ru-SA/C_3N_4	60	24	90	~100	0
	120	6	82	11	89
Ru-NPs/pBN	60	24	42	94	6
	120	6	98	58	42
pBN	60	24	N.R.	N.R.	N.R.
	120	6	N.R.	N.R.	N.R.

Table S5. The structural parameters and the binding energy (E_b) of Ru in different site in DFT calculation

Lattice parameter (Å)			model	Bond	R(Å)	E_b(eV)
Boron nitrogen (BN)	a = 17.587	b = 17.587	c = 20	$Ru-N_2B_2$	Ru-N	1.99	-1.295
					Ru-B	2.15	
				$Ru-N_3$	Ru-N	1.91	-2.383
				$Ru-N_3-V_N$	$Ru-N_1$	1.92	-0.757
					$Ru-N_2$	1.93	
				$Ru-B_2N$	Ru-B	1.95	0.623
					Ru-N	1.87	
				$Ru-B_3$	Ru-B	2.00	0.912
Graphene (NC)	a = 17.278	b = 17.278	b = 20	$Ru-SA/NC-V_C$	$Ru-N_1$	1.92	1.933
					$Ru-N_2$	1.90	
$g-C_3N_4$	a = 21.404	b = 21.404	b = 20	$Ru-SA/C_3N_4$	$Ru-N_1$	2.04	3.529
					$Ru-N_2$	1.92	

Table S6. The adsorption energy of vanillin on different surface in DFT

	model	E_{ads}(eV)
Horizontal vanillin	Ru-SA/h-BN-1	-1.979
	Ru-SA/h-BN-2	-1.903
	Ru-SA/h-BN-3	-1.867
	Ru-SA/h-BN-4	-1.738
	Ru-SA/pBN-V_N-1	-2.108
	Ru-SA/pBN-V_N-2	-2.204
	Ru-SA/NC-V_C-1	-2.011
	Ru-SA/C_3N_4-1	-2.119
Vertical vanillin	Ru-SA/h-BN-5	-1.400
	Ru-SA/pBN-V_N-3	-1.334
	Ru-SA/NC-V_C-2	-1.497
	Ru-SA/C_3N_4-2	-1.189

Table S7. The comparison of catalytic performance between the Ru-SA/BN catalyst and previous reported catalysts.

Catalyst	Temp (℃)	Time (h)	Conv (%)	H_2 (MPa)	Selectivity (%)		Reference
					Vanillyl Alcohol	methoxyphenol	
Ru-SA/BN	60	24	95	4	~100	0	This work
	120	6	~100	4	0	~100	
Ru_1/C_3N_4	60	72	95	4	100	0	*J. Am. Chem. Soc.* 2018, **140**, 11161-11164.
	140	4	100	4	0	100	
Pd/MSMF	90	1	~95	1	46.4	53.6	*J. Mater. Chem. A*, 2013,**1**, 8630-8635
	110	2	~95	1	-	~95	
Ru@GO	25	12	~100	1	~100	0	*Green Chem*., 2020, **22**, 2018
	25	24	~100	1	0	93.2	
Ru/CNTs	50	3	100	1	98	2	*Catalysis Communications,* 2014**, 47**, 28–31
	150	3	100	1	2	96	
Pd@APF-H_2O_2	40	3	100	1	99.5	0.5	Small 2022, **18**, 2106893
	120	2	100	4	0.8	99.2	